

# Muon spectroscopy investigation of anomalous dynamic magnetism in $\text{NiI}_2$

T.L. Breeze<sup>1</sup>, B.M. Huddart<sup>1,2</sup>, A. Hernández-Melán<sup>1</sup>, N.P. Bentley<sup>1</sup>, D.A. Mayoh<sup>3</sup>, G.D.A. Wood<sup>3</sup>, G. Balakrishnan<sup>3</sup>, J. Wilkinson<sup>4</sup>, F.L. Pratt<sup>4</sup>, S.J. Clark<sup>1</sup>, T. Lancaster<sup>1</sup>.

<sup>1</sup>Department of Physics, Center for Materials Physics,  
Durham University, Durham, DH1 3LE, United Kingdom

<sup>2</sup>Clarendon Laboratory, University of Oxford, Department of Physics, Oxford OX1 3PU, United Kingdom

<sup>3</sup>Department of Physics, University of Warwick, Coventry, CV4 7AL, United Kingdom

<sup>4</sup>ISIS Facility, STFC-Rutherford Appleton Laboratory,  
Harwell Science and Innovation Campus, Didcot, OX11 0QX, United Kingdom

(Dated: July 8, 2024)

We present the results of muon-spin relaxation ( $\mu^+\text{SR}$ ) measurements of the van der Waals magnet  $\text{NiI}_2$ , which probe magnetic phase transitions at  $T_{\text{N}1} = 73$  K and  $T_{\text{N}2} = 60$  K. Supporting density functional theory (DFT) calculations allow the determination of a single muon stopping site whose magnetic environment is consistent with the proposed ground-state magnetic structure.  $\mu^+\text{SR}$  measurements of the dynamics reveal behavior consistent with spin-wave excitations below  $T_{\text{N}2}$ , with an additional contribution from a nonmagnetic component of the material. In the region  $T_{\text{N}1} < T < T_{\text{N}2}$  the system is magnetically ordered throughout the bulk, but the character of the dynamics changes qualitatively, resulting in an unusual region of temperature-independent fluctuations.

Magnetic van der Waals materials are two-dimensional (2D) crystals containing magnetic elements, expected to exhibit intrinsic low-dimensional magnetic properties. These cleavable materials provide a platform for exploring magnetism in the 2D limit, where a range of emergent phenomena are expected [1, 2]. Aims in this field include the stabilization of topological spin textures, such as vortices, skyrmions or merons [3], or the realization of novel topological magnetic states of matter, featuring topological order or bandstructures [4, 5].  $\text{NiI}_2$  is a member of the transition-metal dihalides, a family previously noted for multiferroic behavior [6], with  $\text{NiI}_2$  itself displaying ferroelectricity and antiferromagnetic order in its ground state [7]. Recently, it has been proposed that it hosts a novel form of skyrmion phase in the 2D limit [8–10]. Muon spectroscopy is a sensitive probe of low-dimensional magnetism and the dynamics resulting from topological excitations [3, 11, 12]. Here we use the technique to investigate the magnetic transitions in  $\text{NiI}_2$  and the low-temperature magnetic dynamics. The magnetic ground state is shown to be conventional, despite its complicated screw-helical magnetic structure, although we also find evidence for the coexistence of a nonmagnetic component. The regime close to the magnetic ordering temperature is found to have a distinct temperature-independent dynamic signature.

$\text{NiI}_2$  is a centrosymmetric magnetic semiconductor long known for its helimagnetism [7, 13–17]. The material crystallises in the rhombohedral  $\text{CdCl}_2$ -type structure ( $R\bar{3}m$ ) with a magnetic  $\text{Ni}^{2+}$  ion ( $S = 1$ ) carrying an ordered moment of  $1.6\mu_B$  [6, 7]. A single layer of  $\text{NiI}_2$  is characterized by a triangular net of magnetic cations and competing ferromagnetic and antiferromagnetic interactions, resulting in strong magnetic frustration. The static magnetic susceptibility of single crystals show features at  $T_{\text{N}1} = 76$  K and  $T_{\text{N}2} = 58$  K that suggest two successive antiferromagnetic phase transitions in zero applied magnetic field [7]. Evidence of these tran-

sitions is also seen in features in the specific heat capacity [15]. The higher-temperature transition at  $T_{\text{N}1}$  takes the system from a paramagnetic high-temperature phase, to an antiferromagnetic phase on cooling in which, for  $T_{\text{N}2} < T < T_{\text{N}1}$ , the magnetic order comprises ferromagnetic planes coupled antiferromagnetically along the  $c$  axis [7]. At the lower-temperature transition at  $T_{\text{N}2}$  the symmetry of the crystal structure changes from trigonal to monoclinic with decreasing temperature, owing to a slight shift in the Ni layers along the  $a$ -direction giving an overall tilt. This structural distortion causes the spin texture to transform into a screw-helimagnetic ground state with propagation vector  $\mathbf{q} = (0.138, 0, 0.1457)$  in the lattice basis [18]. Here the  $\mathbf{q}$  vector is slanted from the triangular-lattice basal plane and, correspondingly, the spin-spiral plane is also canted from the plane that includes the [001] axis (Fig 1). In the resulting helimagnetic screw-spin ordered ground state,  $\text{NiI}_2$  shows spin-driven ferroelectricity, while the intermediate magnetic state between  $T_{\text{N}1}$  and  $T_{\text{N}2}$  is paraelectric [7].

Magnetically, the transition at  $T_{\text{N}1} = 76$  K has not been investigated in detail, with several earlier studies focusing on the low-temperature multiferroic properties [10, 19–21]. The prediction of skyrmionic spin excitations close to the ordering temperature in monolayers of  $\text{NiI}_2$  motivates this investigation of the ordering behavior of the bulk material and its dynamics at a local level. We present the results of  $\mu^+\text{SR}$  experiments on high-quality single crystal and polycrystalline samples of  $\text{NiI}_2$  along with discussion of the results paired with an analysis of candidate muon stopping sites and the dynamics in the ordered regime. Our results, while being consistent with the reported magnetic ground state of the system, also suggest that the temperature regime  $T_{\text{N}2} < T < T_{\text{N}1}$  is characterized by an unusual spectrum of fluctuations in which the observed muon relaxation is temperature independent and that at temperatures below  $T_{\text{N}2}$  regions of the material exist without an ordered magnetic field,

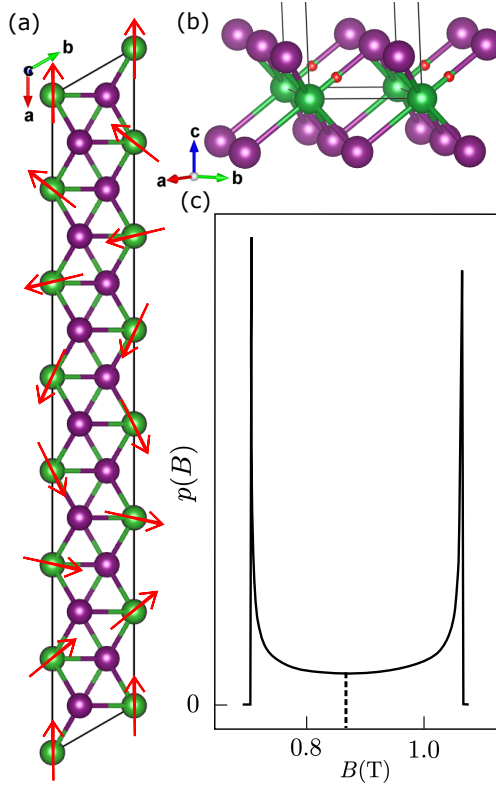


FIG. 1. (a) NiI<sub>2</sub> structure and magnetic ground state showing Ni ions (green) and I ions (purple). The structure comprises stacked trigonal layers of magnetic Ni ions. Arrows indicate spins. (b) Low-energy candidate muon stopping site (red) with (c) the associated field distribution,  $p(B)$ , (arbitrary units) with a mean field of 0.87 T indicated by the dashed line.

probably due to nonmagnetic defects.

We grew single crystals of NiI<sub>2</sub> by the Bridgman method [22]. Stoichiometric quantities of Ni and I were inserted into a quartz tube which was then sealed under vacuum. The tube was inserted into a vertical Bridgeman furnace and slowly heated to 750°C. The tube was then slowly cooled at 1°C/hr to 600°C. Once at 600°C the tube was then rapidly cooled to room temperature and then removed from the furnace. We have characterized our samples by carrying out field-cooled magnetic susceptibility measurements, which is also in agreement with previous results [7].

In a  $\mu^+$ SR experiment spin-polarized muons are implanted in a sample where they interact with the local magnetic field at the muon site. After, on average, 2.2  $\mu$ s, the muons decay into a positron and two neutrinos. By detecting the positrons, which are preferentially emitted in the direction of the muon spin at the time of decay, we can track the polarization of the muon-spin ensemble [23]. In a zero-field (ZF)  $\mu^+$ SR experiment the local magnetic field at the muon sites arises due to the configuration of the spins in the system. When the muon-spin has a component perpendicular to the local field  $B$ , precession occurs with angular frequency  $\omega = \gamma_\mu B$ , where

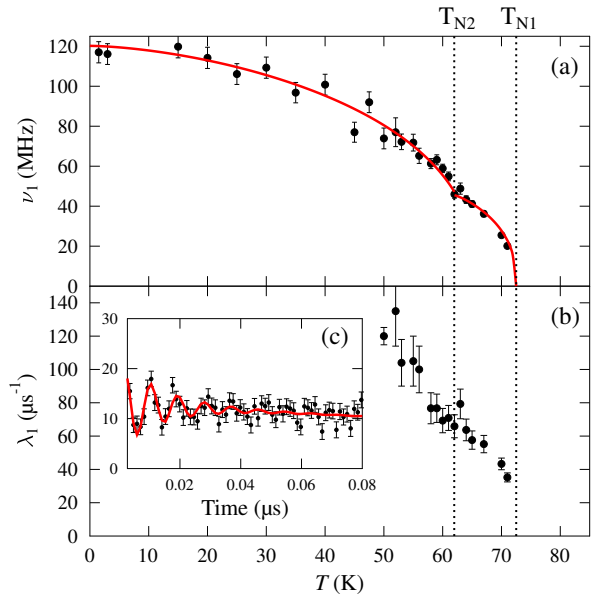


FIG. 2. Temperature evolution of  $\mu^+$ SR fitting parameters (a)  $\nu_1$  and (b)  $\lambda_1$ . Inset: example  $\mu^+$ SR spectrum at 3 K (c) with fit in red, plotted as percentage asymmetry. The frequency  $\nu_1$  in (a) drops to zero at  $T_{N1}$ , indicating the absence of long-range order above this temperature. The transition at  $T_{N2}$  is seen in a discontinuous change in the gradient of  $\nu$ . Red lines are guides to the eye. In (b) the relaxation rate  $\lambda_1$  is fixed at 120  $\mu$ s<sup>-1</sup> in the fitting routine below 50 K.

$\gamma_\mu = 2\pi \times 135.5$  MHz T<sup>-1</sup> is the gyromagnetic ratio of the muon. When the muon-spin aligns with the local field, only dynamic fluctuations can depolarize the muon-spin ensemble. The quantity of interest in the experiment is the asymmetry  $A(t)$ , calculated from counts measured in the detectors forwards and backwards of the initial muon-spin polarization direction  $N_{F,B}$ , corrected using a parameter  $\alpha$  reflecting detector efficiency, via  $A(t) = (N_F - \alpha N_B) / (N_F + \alpha N_B)$ . The asymmetry is directly proportional to the polarization of the muon ensemble. Spectra were fitted using the WiMDA fitting program [24].

We made zero-field (ZF)  $\mu^+$ SR measurements at temperatures from 1.7 K to 80 K using the GPS spectrometer at S $\mu$ S [25], with points concentrated close to the two transitions. Measurements were made on a single crystal sample consisting of a disc of NiI<sub>2</sub> with the  $c$  axis parallel to the initial muon-spin polarization. Below  $T_{N1}$  oscillations are observed in the muon asymmetry, corresponding to long-range magnetic order (LRO) occurring throughout the bulk of the material. We find that a good fit is achieved with only one oscillatory frequency with no phase offset, indicating a dominant contribution to the asymmetry signal from a single muon stopping site. We fit the measured asymmetry to a model of the form

$$A(t) = A_1 e^{-\lambda_1 t} \cos(2\pi\nu_1 t) + A_2 e^{-\lambda_2 t} + A_3, \quad (1)$$

where the first term corresponds to a relaxing precession

of the muon spin components perpendicular to the local magnetic field. Terms two and three are relaxing and constant background components respectively, with the former due to those muon-spin components initially parallel to the internal magnetic field. For our single crystal measurement we find that the ratio  $A_1 : A_2$  is roughly 3:1. Over the range of temperatures up to 72 K the data exhibit very fast damping of the oscillatory term (with the oscillations only visible for roughly the first 0.1  $\mu$ s), while we find  $\lambda_2$  is small compared to  $\lambda_1$ . In fitting the data the relaxing amplitudes  $A_1$  and  $A_2$  are held constant, as is  $\lambda_2$ . Above  $T \approx 72$  K the oscillations are no longer visible. Fig 2 shows plots of the fitted parameters, including frequencies  $\nu_1$  against temperature. The data above 62 K are fitted to a model

$$\nu_1(T) = \nu_0[1 - (T/T_N)^\alpha]^\beta, \quad (2)$$

where  $T_N$  is a critical temperature and  $\nu_1$  is an effective order parameter for the magnetic phase transition. We find  $T_{N1} = 72.5(1)$  K (Fig 2) with exponents  $\alpha = 1.20(1)$  and  $\beta = 0.39(1)$ , fairly typical of a three-dimensional Heisenberg system. At 62 K there is a subtle change in behavior of  $\nu_1$  involving a discontinuous change in the gradient of the measured frequency (Fig 2(a)) corresponding to the transition at  $T_{N2}$ .

We carried out supporting muon-site computations using the MuFinder software [26]. We populate a supercell of the structure with muons at random positions and then carry out a DFT geometry optimization using the CASTEP [27] code to relax the geometry of the full structure, causing muons to fall into local minima of energy. Calculations are done using the PBE functional [28], with a plane wave basis set cut-off energy of 465 eV and a k-point grid of size  $2 \times 2 \times 1$  for a 24 Ni supercell. Following a geometry optimization, muons are grouped into symmetry-equivalent positions so that they can be clustered into similar stopping sites. Our measurements of both the monoclinic ( $T < T_{N2}$ ) and rhombohedral ( $T_{N2} < T < T_{N1}$ ) structures are consistent with a single low-energy stopping site. The minimum energy site for both structural phases is found to occur at the same location, between the Ni ion and the nearest I ion [Fig 1 (b)]. Using this candidate stopping site we can calculate the local dipole field experienced by implanted muons and then construct simulated  $\mu^+$ SR spectra for comparison with the data. The simulated polarization is computed using

$$P_z(t) = \sum_i f_{z,i}^2 p_i + \sum_i (1 - f_{z,i}^2) p_i \cos(\gamma_\mu B_i t), \quad (3)$$

where the probabilities  $p_i$  correspond to occupancies of different muon sites,  $B_i$  is the magnitude of the local field and  $f_{z,i} = B_{z,i}/B_i$  is the computed ratio of the  $z$  component of magnetic field to the overall local field magnitude.

The low-temperature magnetic ground state is predicted to be helimagnetic with a spin spiral with a com-

ponent along the  $a$  axis that results in one complete rotation of the spin across roughly seven unit cells [7, 19], described by the spin propagation vector (0.138, 0, 0.1457). Computing the resulting local dipole field with an ordered Ni ion moment of  $1.6\mu_B$  [6] at the predicted low-energy muon site yields a distribution of fields felt by muons in structurally equivalent but magnetically inequivalent sites [Fig 1(c)]. This distribution shows two prominent peaks, and a simulated spectrum is therefore dominated by oscillations at two frequencies with associated fields corresponding to the peaks. However, our muon site calculations indicate that there is a very shallow local minimum in energy about the candidate site, and a large number of sites with small displacements (all within 0.4 Å of each other) from the average are found in the calculation. Averaging over the dipole field contributions from each of these sites broadens the two peaks such that they overlap, resembling a single gaussian peak centred on the average field at the muon of 0.867 T, equivalent to a precession frequency of 117 MHz. This frequency is in good agreement with our single measured frequency close to  $T = 0$  K. Finally, calculating a simulated zero temperature spectrum from this distribution and applying the same fitting function used for the data gives a crude estimate for the relaxation of  $\lambda_1 = 175 \mu\text{s}^{-1}$ . Compared to our experimental value of  $\lambda_1 = 120 \mu\text{s}^{-1}$ , this suggests that the relaxation in the oscillating component is accounted for by decoherence due to this distribution of local fields, with relatively little dynamic contribution. Spin-DFT calculations in other work on this material suggests that the magnetic ground state is complicated by a magnetisation of the I nuclei by the Ni ions [19]. We found, however, that we were able to produce simulated spectra that agreed well with experiment assuming magnetic centres on the Ni nuclei only.

In the intermediate temperature regime  $T_{N2} < T < T_{N1}$ , the magnetic structure is predicted to be a simple antiferromagnet with the spin propagation vector (0, 0, 1/2). A similar dipole field analysis in this case gives an average field of 0.695 T, corresponding to a 0 K precession frequency of 93 MHz for this structure. An extrapolation of the fitted frequency data in this region with the order parameter fit described above suggests a 0 K frequency of 92 MHz, in good agreement with this theoretical value, though it should be noted that this fit is not strongly constrained by the small number of data points in this region.

We carried out further measurements on a polycrystalline sample using the HiFi instrument (STFC-ISIS Facility) [29], which allows for observation of the longer-time behavior in order to probe dynamics. ZF measurements were made across the same temperature interval as for the single-crystal measurements. In this case the oscillations are not resolvable as they occur over too short a period compared to the ISIS pulse width. Asymmetry spectra were therefore fitted to the function

$$A(t) = A_4 e^{-\lambda_4 t} + A_5, \quad (4)$$

with  $A_5$  held constant at 13.6%, from which an initial asymmetry  $A_0 [= A(t = 0)]$  can be calculated for each temperature via  $A_0 = A_4 + A_5$ . Results of the fitting procedure are shown in Fig 3. We see indications of phase transitions at both  $T_{N1}$  and  $T_{N2}$ , with  $A_0$  undergoing a broad drop at  $T_{N2} \approx 58$  K followed by a sharp increase at  $T_{N1} \approx 73$  K.

We would expect the high temperature data ( $T > T_{N1}$ ) to include the full relaxing asymmetry  $A_{\text{rel}}$  resulting from all muons implanted in the sample, excluding background contributions. In a fully-ordered magnetic state we expect to see only 1/3 of the relaxing asymmetry resulting from muon spins initially parallel to the local field. The remaining 2/3, corresponding to spin-components initially perpendicular to the local field, result in non-resolved oscillations. Notably, in the intermediate region  $T_{N2} < T < T_{N1}$ , 1.4% of asymmetry is lost, which implies that new relaxation channels are accessed in this regime that were not active below  $T_{N2}$ . In fact, this is consistent with the single crystal data, in which a fit with oscillating amplitude,  $A_1$ , allowed to vary over short times leads to a slight increase in  $A_1$  above  $T_{N2} = 58$  K, consistent with a greater fraction of the sample being magnetic.

Our proposed explanation for the observed behaviour is therefore that the system is fully magnetically ordered only in the region  $T_{N2} < T < T_{N1}$ , while, in the region  $T < T_{N2}$  there are contributions from some muon sites in regions without an ordered field. Such regions might result from states near the surfaces of the crystal or, perhaps more likely, from domain-wall like regions or other defects in the magnetic structure such as stacking faults. Assuming the material is completely ordered in the intermediate temperature regime, the asymmetry at these temperatures should be equal to 1/3 of the total relaxing asymmetry which is observed in the totally disordered phase above  $T_{N1}$ , accounting for some background asymmetry. We estimate that the disordered fraction of the sample below  $T_{N2}$  is 15% by volume. This is computed assuming a total relaxing asymmetry  $A_{\text{rel}} = 12\%$  and low temperature magnetic and nonmagnetic contributions  $A_{\text{mag}}^{\text{low}} = 10.2\%$  and  $A_{\text{nonmag}}^{\text{low}} = 1.8\%$  respectively.

The dynamic signature of the magnetism is accessible via the longitudinal relaxation rate  $\lambda_4$ , which rises approximately linearly up to a broad peak, which occurs  $\approx 10$  K below  $T_2$ . The rate  $\lambda_4$  then falls to a constant value in the region between transitions, before increasing to a second peak at 73 K. Such dynamics peaks are often indicative of local field fluctuation rates that decrease close to magnetic transitions. Below  $T_{N2}$  the evolution of  $\lambda_4(T)$  is consistent with the fluctuations from spin-wave excitations in the case of a single gapless magnon band [30–32], for which we expect  $\lambda \propto T^p$ . We obtain a good fit to the data below 50 K with  $p = 1$ , where

$$p = \frac{2D}{s} - 1. \quad (5)$$

Here  $D$  is the effective dimensionality (which we expect to be 1 here since the magnetic structure is described by

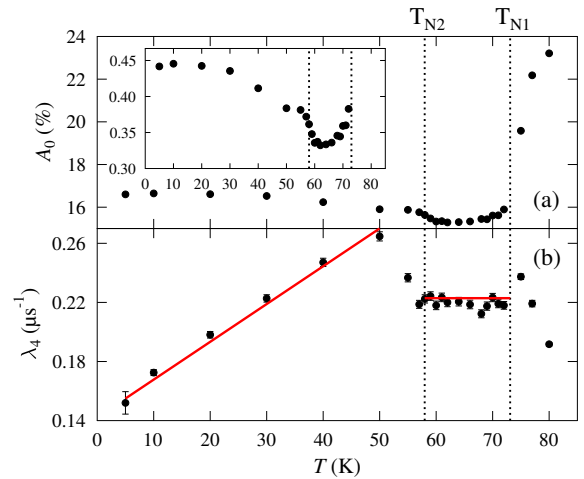


FIG. 3. Temperature evolution of parameters from fits to Eq. 4. (a) Initial asymmetry,  $A_0 = A(t = 0)$  (inset:  $A_0$  in the region  $14.9\% \leq A_0 \leq 16.9\%$  plotted as a fraction of  $A_{\text{rel}}$ ) and (b) relaxation rate  $\lambda_4$  with power law fits in different regions.

a single propagation vector) and  $s = 1$  is the exponent for the spin wave dispersion relation  $\omega = q^s$ . Our exponent  $p = 1$  is consistent with  $s = D = 1$ , corresponding to the helimagnetic magnetic structure predicted. This implies that the dynamics in this range are well described by contributions from a single magnon band that dominates the magnetic excitations.

In the intermediate temperature region  $T_{N2} < T < T_{N1}$ , we again expect  $s = 1$ , owing to the simple antiferromagnetic spin texture. However, here the data suggests  $p = 0$ , which cannot be satisfied for integer  $D$ . This suggests that above 60 K the dynamics we detect through the relaxation rate  $\lambda_4$  are qualitatively different from those for  $T < T_{N2}$ , and can no longer be described by a single gapless magnon band. It is possible that paraelectric fluctuations in this region complicate the observed dynamics, but the nature of the dynamics in this range are not made clear by our muon spectroscopy measurements.

In conclusion, muon-spin spectroscopy measurements have shown features corresponding to two successive phase transitions at  $T_{N1} \approx 73$  K and  $T_{N2} \approx 60$  K. With the addition of a DFT muon stopping site analysis we have been able to identify a muon site located between neighbouring Ni and I ions, whose behavior is consistent with the proposed magnetic structure, assuming we allow a small variation in the location where the site is realized. A notable feature is the presence of a nonmagnetic component for  $T < T_{N2}$ , probably due to nonmagnetic defects forming 15% of the sample by volume. The dynamic relaxation shows a linear increase in the region below 58 K, followed by a constant region between transitions, indicative of a qualitative change in excitation spectrum, which coincides with the change in magnetic structure. It is worth noting that the prediction of skyrmions in a monolayer of this material was for a phase occurring at

temperatures close to the ordering temperature, where skyrmions were presumably stabilized by thermal fluctuations. Given that we have identified two regimes of dynamics, it will be interesting in the future to see whether either region is able to support the equilibrium occurrence of skyrmion excitations in applied magnetic field in samples formed from a limited number of layers.

Muon measurements were made at the Swiss Muon Source and the STFC-ISIS Facility and we are grateful for the provision of beamtime. We also thank Chen-

nan Wang and Hubertus Luetkens ( $S\mu S$ ) for their assistance over the course of these measurements. Computational work was done using the Hamilton8 HPC service of Durham University and the ARCHER2 UK National Supercomputing Service (<https://www.archer2.ac.uk>). We acknowledge support from EPSRC (UK) (grant numbers: EP/N032128/1, EP/X035891/1 and EP/T005963/1 and T.L.B's studentship). N.P.B is grateful for the support of the Durham Doctoral Scholarship. Data will be made available via DOI:XXXXXXXXXX.

---

[1] K.S. Burch, D. Mandrus, and J. Park. *Nature* **563**, 47 (2018).

[2] Q.H. Wang, A. Bedoya-Pinto, M. Blei, A.H. Dismukes, A. Hamo, S. Jenkins, M. Koperski, Y. Liu, Q. Sun, E.J. Telford, et al. *ACS nano* **16**, 6960 (2022).

[3] T. Lancaster. *Contemp. Physics* **60**, 246 (2019).

[4] S. Kezilebieke, M.N. Huda, V. Vaňo, M. Aapro, Somesh C. Ganguli, O.J. Silveira, S. Głodzik, A.S. Foster, T. Ojanen, and P. Liljeroth. *Nature* **588**, 424 (2020).

[5] G. Zhang, H. Wu, L. Zhang, L. Yang, Y. Xie, F. Guo, H. Li, B. Tao, G. Wang, W. Zhang, et al. *Small* **18**, 2204380 (2022).

[6] M.A. McGuire. *Crystals* **7**, 121 (2017).

[7] T. Kurumaji, S. Seki, S. Ishiwata, H. Murakawa, Y. Kaneko, and Y. Tokura. *Phys. Rev. B* **87**, 014429 (2013).

[8] D. Amoroso, P. Barone, and S. Picozzi. *Nat. Commun.* **11**, 5784 (2020).

[9] M. Blei, J.L. Lado, Q. Song, D. Dey, O. Erten, V. Pardo, R. Comin, S. Tongay, and A.S. Botana. *Appl. Phys. Rev.* **8**, 021301 (2021).

[10] Q. Song, C.A. Occhialini, E. Ergeçen, B. Ilyas, D. Amoroso, P. Barone, J. Kapeghian, K. Watanabe, T. Taniguchi, A.S. Botana, et al. *Nature* **602**, 601 (2022).

[11] T. Lancaster, F. Xiao, Z. Salman, I.O. Thomas, S.J. Blundell, F.L. Pratt, S.J. Clark, T. Prokscha, A. Suter, S.L. Zhang, et al. *Phys. Rev. B* **93**, 140412 (2016).

[12] M.N. Wilson, T.J. Hicken, M. Gomilšek, A. Štefančič, G. Balakrishnan, J.C. Loudon, A.C. Twitchett-Harrison, F.L. Pratt, M. Telling, and T. Lancaster. *Phys. Rev. B* **104**, 134414 (2021).

[13] P. Day, A. Dinsdale, E.R. Krausz, and D.J. Robbins. *Journal of Phys. C* **9**, 2481 (1976).

[14] P. Day and K.R.A. Ziebeck. *Journal of Phys. C* **13**, L523 (1980).

[15] D. Billerey, C. Terrier, N. Ciret, and J. Kleinclauss. *Phys. Lett. A* **61**, 138 (1977).

[16] J. Kapeghian, D. Amoroso, C.A. Occhialini, L.G.P. Martins, Q. Song, J.S. Smith, J.J. Sanchez, J. Kong, R. Comin, P. Barone, et al. *Phys. Rev. B* **109**, 014403 (2024).

[17] H. Liu, X. Wang, J. Wu, Y. Chen, J. Wan, R. Wen, J. Yang, Y. Liu, Z. Song, and L. Xie. *ACS nano* **14**, 10544 (2020).

[18] S.R. Kuindersma, J.P. Sanchez, and C. Haas. *Physica B + C* **111**, 231 (1981).

[19] A.O. Fumega and J.L. Lado. *2D Mater.* **9**, 025010 (2022).

[20] H. Ju, Y. Lee, K. Kim, I.H. Choi, C.J. Roh, S. Son, P. Park, J.H. Kim, T.S. Jung, J.H. Kim, et al. *Nano letters* **21**, 5126 (2021).

[21] D. Lebedev, J.T. Gish, E.S. Garvey, T.K. Stanev, J. Choi, L. Georgopoulos, T.W. Song, H.Y. Park, K. Watanabe, T. Taniguchi, et al. *Adv. Func. Mater.* **33**, 2212568 (2023).

[22] M. Yoshinaga, T. Iida, M. Noda, T. Endo, and Y. Takanashi. *Thin Solid Films* **461**, 86 (2004).

[23] S. Blundell, R. De Renzi, T. Lancaster, and F.L. Pratt. *Muon Spectroscopy: An Introduction*. Oxford University Press, (2022).

[24] F.L. Pratt. *Physica B* **289**, 710 (2000).

[25] A. Amato, H. Luetkens, K. Sedlak, A. Stoykov, R. Scheuermann, M. Elender, A. Raselli, and D. Graf. *Review of Scientific Instruments* **88**, (2017).

[26] B.M. Huddart, A. Hernández-Melián, T.J. Hicken, M. Gomilšek, Z. Hawkhead, S.J. Clark, F.L. Pratt, and T. Lancaster. *Comp. Phys. Commun.* **280**, 108488 (2022).

[27] S.J. Clark, M.D. Segall, C.J. Pickard, P.J. Hasnip, M.I.J. Probert, K. Refson, and M.C. Payne. *Zeitschrift für kristallographie-crystalline materials* **220**, 567 (2005).

[28] J.P. Perdew, K. Burke, and Y. Wang. *Phys. rev. B* **54**, 16533 (1996).

[29] P.J.C. King, R. de Renzi, S.P. Cottrell, A.D. Hillier, and S.F.J. Cox. *Physica Scripta* **88**, 068502 (2013).

[30] M. Gomilšek, T.J. Hicken, M.N. Wilson, K.J.A. Franke, B.M. Huddart, A. Štefančič, S.J.R. Holt, G. Balakrishnan, D.A. Mayoh, M.T. Birch, S.H. Moody, H. Luetkens, Z. Guguchia, M.T.F. Telling, P.J. Baker, S.J. Clark, and T. Lancaster. *arXiv preprint arXiv:2312.17323* (2024).

[31] D. Beeman and P. Pincus. *Phys. Rev.* **166**, 359 (1968).

[32] N. Janša, A. Zorko, M. Gomilšek, M. Pregelj, K.W. Krämer, D. Biner, A. Biffin, C. Rüegg, and M. Klanjšek. *Nature physics* **14**, 786 (2018).